Structural and electrical properties of an Au film system deposited on silicone oil surfaces

2002 J. Phys.: Condens. Matter 14 10051

(http://iopscience.iop.org/0953-8984/14/43/304)

INSTITUTE OF PHYSICS PUBLISHING JOURNAL OF PHYSICS: CONDENSED MATTER

J. Phys.: Condens. Matter **14** (2002) 10051–10062 PII: S0953-8984(02)35553-X

Structural and electrical properties of an Au film system deposited on silicone oil surfaces

Bo Yang, A-Gen Xia, Jin-Sheng Jin, Quan-Lin Ye, Yan-Feng Lao, Zheng-Kuan Jiao and Gao-Xiang Ye

Department of Physics, Zhejiang University, Hangzhou 310028, People's Republic of China

Received 5 April 2002, in final form 9 August 2002
Published 18 October 2002
Online at stacks.iop.org/JPhysCM/14/10051

Abstract

An Au thin film system, deposited on silicone oil surfaces by the thermal deposition method, has been fabricated and its structure as well as electrical properties has been studied. A web-shaped characteristic surface morphology of the films is observed. The dc sheet resistance R of the metal films on the liquid surfaces is measured during and after deposition *in situ* by the four-probe method. The time dependence of the sheet resistance can be explained in terms of the film growth mechanism on the oil surface. The anomalous I–V characteristics of the film system can be interpreted as a competition among the local Joule heating, hopping and tunnelling effects. It is found that the dc third-harmonic coefficient B_0 and the zero-power resistance R_0 satisfy the power-law relation $B_0 \propto R_0^{2+w}$ and the exponent w is close to zero. This result indicates that the hopping and tunnelling effects in the samples are much stronger than those of the other film systems. We also find $I_m \propto R_0^{-\beta}$ with $\beta = 0.79 \pm 0.08$ and $I_m \propto B_0^{-\gamma}$ with $\gamma = 0.49 \pm 0.07$, where I_m is the critical current. The physical origins of the phenomena are discussed.

1. Introduction

The experimental and theoretical works of metal thin films were reported extensively in the past half centuries [1, 2]. People have begun to truly understand the structure and physical properties (mechanical, electrical, magnetic, optical etc) of metal thin films on solid substrates. Structurally, these films normally can be produced in two different forms, flat and rough film systems [3–9]. It is well known that the nature of the substrates as well as the deposition method plays a significant role in both microstructure and physical properties of thin film systems [8, 10–12]. For instance, the bilateral rough film system, which can be fabricated by using rough substrates, exhibits a characteristic percolation structure and anomalous electrical behaviours, indicating the physical mechanism of electrical process in this system is quite different from that of the percolation films deposited on flat solid substrates [12].

The microstructure of a percolation film can be considered as a random resistance network with total sheet resistance R, carrying a current I, which is made up of elements of resistances r_a carrying currents i_a. The theoretical analysis of this random resistor network (RRN) model gives [13, 14]

$$B \propto R_0^{2+w}, \tag{1}$$

where R_0 is the zero-power sheet resistance, w is a critical exponent, which is sensitive to the microstructure of the film, and B is the normalized third-harmonic coefficient, which is closely related to both the $1/f$ noise spectrum and the breakdown current of the system. The dc third-harmonic coefficient B_0, which equals the value of B when the frequency of the current approaches zero, is obtained from the dc R–I relation of the films [11–14]

$$R = R_0 + B_0 I^2. \tag{2}$$

This quadratic R–I behaviour is generally explained in terms of the rise in temperature of the hot spots (or links) in the film due to the local Joule heating, but the microstructure of the percolation film remains unchanged [14]. Above the percolation threshold P_c, the breakdown current I_c and R_0 satisfy the power-law relation [12, 14]

$$I_c \propto R_0^{-\alpha}, \tag{3}$$

where I_c is defined as the current at which a hot spot reaches the melting temperature. The critical exponent α is generally considered to be nonuniversal [12, 14–16]. The power-law relation between I_c and B, i.e.,

$$I_c \propto B^{-x}, \tag{4}$$

is found [14]. It is reported that the critical exponent x is almost insensitive to the microstructure of the films [14].

Recently, the structure and growth mechanisms of metal films deposited on liquid substrates by thermal deposition are studied [17–20]. Aggregate structures were formed, which could be identified at ambient or vacuum conditions by optical microscopy. It was found that such aggregates are confined to the oil surface and perform Brownian motion on the oil surface. Experimental results show that the structure and growth mechanism of this kind of film system are quite different from those of the other film systems deposited on solid substrates [8–14]. Unfortunately, since the film structures formed on the liquid surfaces are movable and unstable due to the fluidity of the liquid substrates, it is very difficult to experimentally study the physical properties of these film systems.

In this paper, we present the surface morphology and electrical properties of Au films deposited on silicone oil surfaces by the thermal deposition method. A special approach for the investigation of the electrical properties of metal thin films on a liquid surface is chosen. The dc sheet resistance R of these films is measured *in situ* during and after deposition by the four-probe method. It is found that the resistance R strongly depends on the deposition time and aggregation time. These resistance behaviours can be interpreted in terms of the film growth mechanism on the oil surfaces. The nonlinear dc I–V characteristics are very different from those of the other film systems [13, 14], indicating that the hopping and tunnelling effects in this system are much stronger than those of the other films. The discussion of the power-law behaviours of dc third-harmonic coefficient and critical current is also presented.

2. Experiment

The samples were fabricated by thermal evaporation of 99.9% pure gold in a vacuum of 1.0×10^{-3} Pa. The deposition rate for all samples was 0.25 Å s^{-1}, which was determined by a

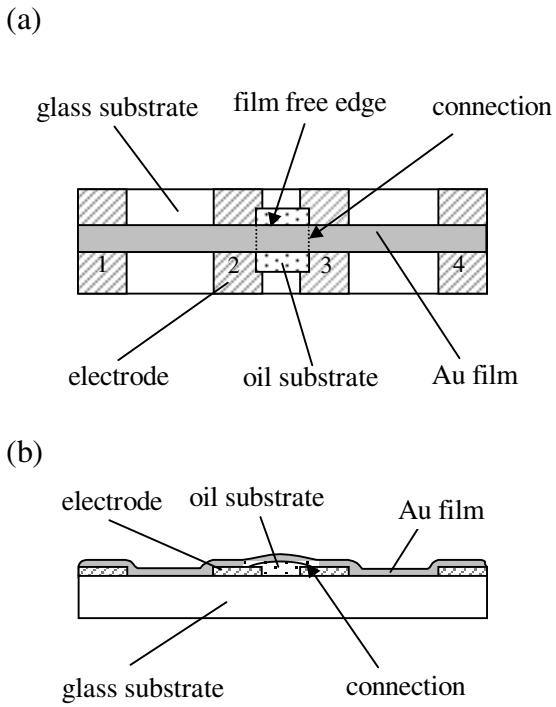

Figure 1. Schematic of the substrate components. (a) is the top view and (b) is the side view. The hatched areas are electrodes 1, 2, 3 and 4. The dotted and shaded areas are the silicon oil substrate and deposited Au film, respectively. The free edge of the Au film on the oil surface and the connection between the Au film on the oil surface and the Au film on the electrode are also shown, respectively.

quartz crystal balance. The nominal deposited film thickness was in the range of 130–550 Å. The deposition was performed at room temperature, i.e., at $(23 \pm 2)\,^{\circ}\mathrm{C}$. The film surface morphologies were characterized with an optical microscope after the samples were removed from the evaporation chamber.

In order to measure the dc sheet resistance R *in situ*, four pieces of Au films 400 Å thick, which are used as electrodes 1, 2, 3 and 4, were deposited on a glass substrate first and the size of the electrodes is $15.0 \times 5.0\ \mathrm{mm}^2$ (see figure 1). Then commercial silicone oil (Dow Corning 705 diffusion pump fluid) with a vapour pressure below 10^{-8} Pa was carefully painted onto the area between and on the two middle electrodes, i.e., electrodes 2 and 3 (see figure 1). It should be mentioned that electrode 2 is very close to electrode 3 (the distance between them is about 0.5 mm) to prevent the oil layer from dewetting the smooth glass surface. The size of the resulting oil substrate is $8.0 \times 4.0\ \mathrm{mm}^2$ with thickness of $\approx$0.5 mm. The metal atoms were deposited on the oil surface, electrodes and the remaining area of the glass substrate at the same time. A shutter with a slit of 3 mm width was mounted over the substrate, which shaped the size of Au films on the oil surfaces (about $4.0 \times 3.0\ \mathrm{mm}^2$) and resulted in good connects between the films and the electrodes (see figure 1). The time dependence of the dc sheet resistance R was measured by the four-probe method during and after deposition. In the resistance measurement, we keep the dc voltage V between electrodes 1 and 4 (see figure 1) constant, i.e., $V = 1$ V, during the measurement. Two days later, after R approached an approximate stable value, the dc I–V characteristics of the samples were measured systematically. All the electrical properties are measured under vacuum conditions.

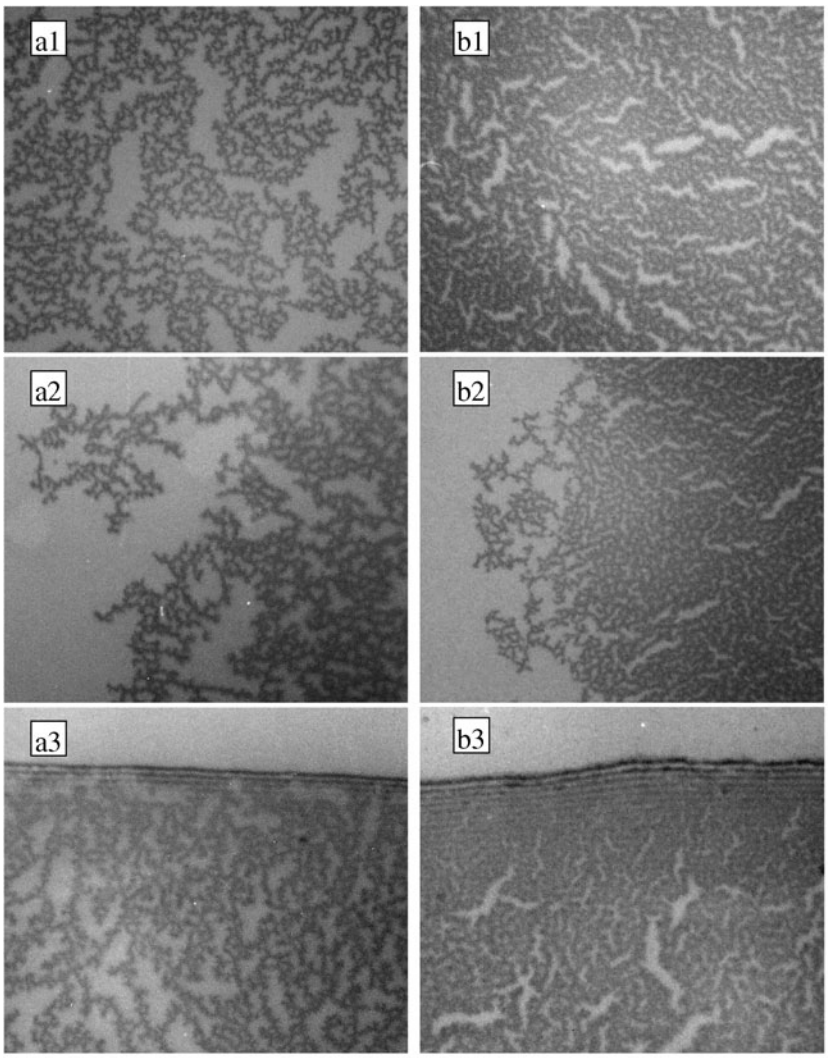

Figure 2. Surface morphologies of two different Au films (dark areas). Image sizes are 105 μm $\times$ 90 μm. The film thicknesses described in (a1), (a2) and (a3) are 130 Å and the film thicknesses in (b1), (b2) and (b3) are 220 Å. (a1) and (b1) show the surface morphologies of the two Au films deposited on the oil surfaces; (a2) and (b2) show the surface morphologies of the free edges of the two films; (a3) and (b3) show the surface morphologies of the connections between the Au films on the oil surfaces (web-shaped parts) and the Au films on electrodes (uniform regions) of the two samples.

3. Results and discussion

Figure 2 shows the images of two Au thin films, with different film thicknesses, deposited on silicone oil surfaces and taken after the electrical measurement, i.e., two days after deposition, in which two-dimensional percolation (web-shaped) structures are observed. We find that, as the film thickness increases, the surface coverage increases and the web-shaped structure films become more compact. However, the branch width of the web-shaped films, which is about 1.2 μm, is independent of the film thickness. This phenomenon is similar to that of the Au

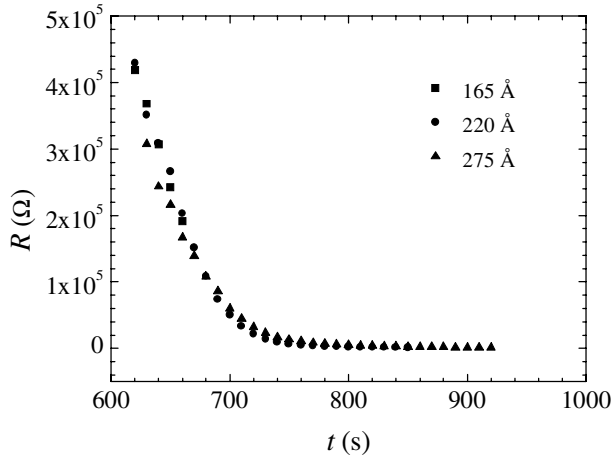

Figure 3. Dependence between the dc sheet resistance R and deposition time t for three samples with thicknesses of 165 Å (squares), 220 Å (circles) and 275 Å (triangles).

films deposited on melting glass surfaces [19]. The surface morphologies of the free edges (see figure 1) of the two films on the oil surfaces are shown in figures 2(a2) and (b2). One finds that the film structures near the free edges are less compact than other parts of the films. Figures 2(a3) and (b3) show the surface morphologies of the connections (see figure 1) between the films on the oil surfaces and the films on the electrodes. The optical interference fringes in figures 2(a3) and (b3) result from the edges of the oil substrates with a wedge-shaped structure on the electrode surfaces (see figure 1). It is observed that the film structures (figures 2(a3) and (b3)) near connections are more compact than other parts of the films, which indicates that the films and the electrodes are connected tightly. In fact, we find in our experiment that these connections are excellent ohmic electrodes for the dc sheet resistance measurements *in situ* for the samples.

The dependence of the dc sheet resistance R on the deposition time t for three different samples is shown in figure 3. It should be mentioned that the upper limitation of the resistance which can be measured in our experiment is around 10^6 Ω. Therefore, after 600 s deposition, the film thickness approaches 130 Å and then the value of the resistance R starts to be detectable. As soon as R becomes detectable, we find that R drops rapidly with the time t. The absolute values of $\mathrm{d}R/\mathrm{d}t$ for the three samples, i.e., $|\mathrm{d}R/\mathrm{d}t|$, in figure 3 are around $6 \times 10^3\ \Omega\ \mathrm{s}^{-1}$. Then, with further increase of the time t, $|\mathrm{d}R/\mathrm{d}t|$ decreases quickly and approaches zero gradually.

We propose that this resistance behaviour can be explained in terms of the metal film growth mechanism on the liquid substrates [17, 18, 20]. During deposition, the deposited Au atoms nucleate on the oil surface first and then compact clusters are formed due to random walk and adhesion upon impact. These Au clusters also perform random motion because of the impact between the liquid molecules and the Au clusters. Therefore, the compact clusters aggregate gradually, which results in ramified Au aggregates on the liquid surfaces. If the deposition continues, these aggregates capture deposited atoms and small compact clusters during their random motion, which results in further growth of the ramified aggregates. With the further increase of the deposition time, the ramified aggregates start to connect with one another. When time t approaches 600 s, the deposited material is enough and most of the ramified aggregates are connected. Therefore, a continuous web-shaped structure forms and the resistance R can be probed. The density of the web-shaped film increases with time t and

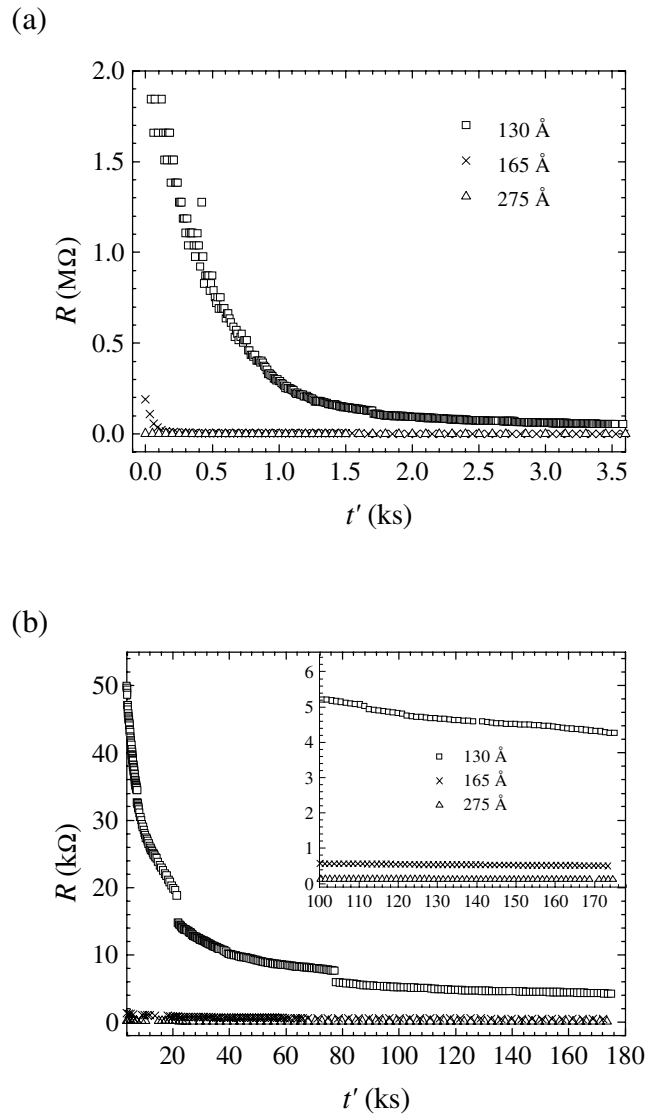

Figure 4. Dependence between the dc sheet resistance R and aggregation time t' for three samples with thicknesses of 130 Å (squares), 165 Å (crosses) and 275 Å (triangles). In (a) the aggregation time t' ranges from 0 to 3.6 ks, in (b) the time t' ranges from 3.6 to 180 ks and in the inset it ranges from 100 to 180 ks.

the resistance R drops quickly. Finally, after all the ramified clusters connect stably, the value of $|\mathrm{d}R/\mathrm{d}t|$ approaches zero (figure 3). One finds in figure 3 that, for the fixed deposition rate, there is approximately no difference among the R–t behaviours of the three different samples, indicating that the R–t behaviour of the samples is repeatable.

After deposition, we measure the dependence between the dc sheet resistance R and aggregation time t'. Figure 4 shows the R–t' behaviour for three samples with different film thicknesses. One finds in figure 4 that the resistance R continues to drop quickly after deposition. As soon as the deposition finishes, the absolute values of $\mathrm{d}R/\mathrm{d}t'$ for the three samples in figure 4(a) are around 4.0×10^3, 2.0×10^3 and $6.0\ \Omega\ \mathrm{s}^{-1}$, respectively, and

decrease with the time t'. Finally, $|\mathrm{d}R/\mathrm{d}t'|$ approaches zero and R approaches a stable value (see figure 4(b)). The stable value of the resistance R strongly depends on the film thickness. The thinner the sample is, the larger the stable value of the resistance will be.

We suggest that this resistance behaviour mainly results from the effects of both the liquid substrate and the characteristic microstructure of the samples. In fact, after deposition, the film is composed of the characteristic web-shaped structure and a huge number of free ramified aggregates which are unconnected. The resistance R decreases rapidly with time t' mainly for two reasons:

(1) the number of the defects in the web-shaped film decrease with t' and the relaxation time should be more than several hours [21], and
(2) again due to the random walk and adhesion upon impact, the free ramified aggregates continue to grow with time t' [17–20] and finally they connect to the web-shaped structure film, which increases the area of the web-shaped film. After all the ramified aggregates connect to the web-shaped film, the resistance R then approaches a stable value (figure 4(b)).

Since the increasing of the film thickness will result in the decrease of the defects and ramified aggregates and increase of the area of the web-shaped film, the structure of the Au films becomes more compact as the film thickness increases. In other words, for a certain aggregation time, as the film thickness increases, the value of $|\mathrm{d}R/\mathrm{d}t'|$ decreases gradually, which is in good agreement with our experimental observations (see figure 4(a)).

In figure 4, the measurement result for the sample 130 Å thick shows some resistance jumps. As discussed above, the decrement of the film thickness will decrease the area of the web-shaped film. Therefore, after deposition, the free ramified aggregates continue to grow with time due to random motion and adhesion upon impact and huge ramified aggregates may be formed in thinner samples. When one of these huge ramified aggregates connects to the web-shaped structure film, the area of the web-shaped film decreases suddenly and hence the resistance R jumps down immediately.

After the dc sheet resistance R approaches an approximate stable value, i.e., two days after deposition, we systematically measure the I–V characteristics of the samples, which is shown in figure 5(a). At low currents it shows ohmic behaviour, i.e., R is a constant. At higher currents, however, the sheet resistance R increases with the current I, which can be well fitted by equation (2). In figure 5(a), we find the dc third-harmonic coefficient $B_0 = (7.28 \pm 0.07) \times 10^3$ V A^{-3}. The quadratic nonlinear response, which is similar to those of the other percolation film systems [11–14], is generally interpreted in terms of a heating and melting process of the hot spots (or links) due to the local Joule heating [14]. This result again provides evidence that the Au films deposited on the oil surfaces exhibit the percolation structure. When the current further increases and goes beyond the critical current I_m, which corresponds to the maximum resistance R_{max}, the resistance drops with the current I, i.e., $\mathrm{d}R/\mathrm{d}I < 0$, which is quite different from the other percolation films [13, 14].

The coefficient B_0 of different samples with different dc sheet resistance R_0 is obtained by fitting the experiment data by equation (2). The scaling of B_0 as a function of R_0 is shown in figure 5(b). The straight line yields a power-law dependence $B_0 \propto R_0^{2+w}$, indicating that the critical exponent w is close to zero. This value of w is much lower than the exponents of the other films and the theoretical predications in a two-dimensional system [13], which indicates that the conductivity of the samples is not purely metallic.

According to the measured result, we suggest that the lower critical exponent w and the anomalous I–V characteristics result mainly from the effects of both the liquid substrates and the characteristic microstructure of the samples because other film systems do not exhibit such

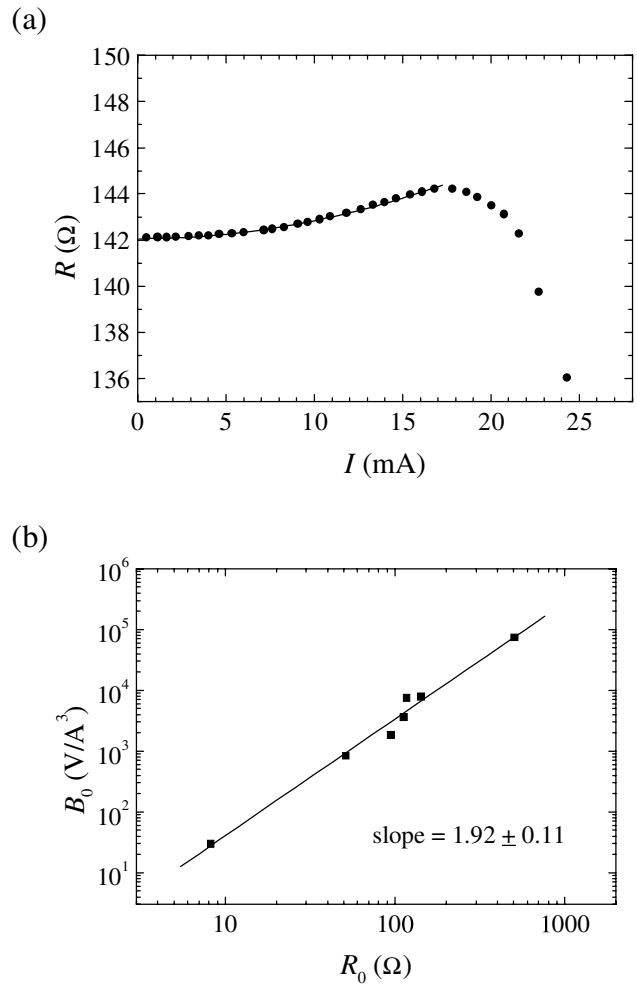

Figure 5. (a) R–I characteristics of the sample 220 Å thick. Circles are the experimental data and the solid line represents the fit $R = R_0 + B_0 I^2$ with $B_0 = (7.28 \pm 0.07) \times 10^3$ V A^{-3}. (b) The scaling of B_0 for the Au film deposited on the silicon oil surface is $2 + w = 1.92 \pm 0.11$, indicating that w is close to zero.

behaviours [13]. As shown in figure 2, the Au films on the oil surfaces exhibit web-shaped structures and therefore a huge number of defects would exist in the films. In other words, many weak links, just like various metal–insulation–metal (MIM) tunnelling junctions, are constructed in the films. When a high current passes through a weak link, the local temperature change is sufficient to excite local hopping and breakdown of the MIM tunnelling junction. Both the tunnelling and hopping effects would reduce the current density of the link and the sheet resistance. The higher the current is, the more the resistance will be reduced, which leads to a weaker third-harmonic component and hence the critical exponent w becomes smaller than that of the other film systems [13]. According to this analysis, the lower critical exponent w indicates that the hopping and tunnelling effects in the samples are much stronger than those of the other films. This conclusion is very reasonable since the weak links or tunnelling junctions in the samples are much more plentiful than in other film systems and the film microstructures are different from the other films [13].

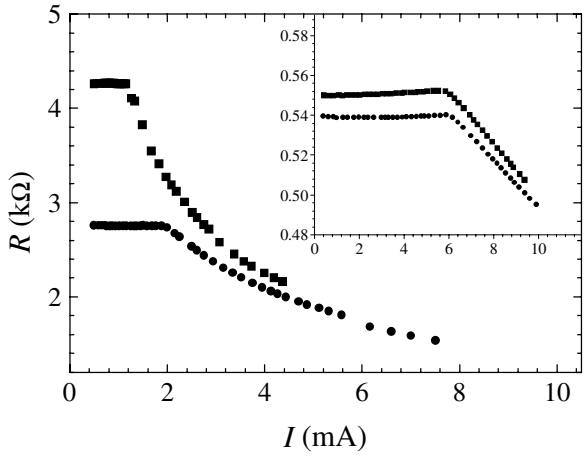

Figure 6. R–I characteristics of the sample of 130 Å thickness. Squares and circles represent the first and the second R–I measured results, respectively. The inset shows the R–I characteristics of the sample of 165 Å thickness.

We propose that the anomalous R–I characteristics of the Au samples are caused by a competition among the local Joule heating, tunnelling and hopping effects. At low current, the local Joule heating effect is the main contribution to the electrical process, which results in the phenomena of $\mathrm{d}R/\mathrm{d}I > 0$ and $\mathrm{d}R/\mathrm{d}I$ increasing with I. Then the tunnelling and hopping effects strengthen with the current, which leads to $\mathrm{d}R/\mathrm{d}I$ decreasing, although the local Joule heating effect is still active at that time. When $I = I_m$, the local Joule heating effect equals the tunnelling and hopping effects and hence the resistance R reaches the maximum value R_{max}. If $I > I_m$, the tunnelling and hopping effects are the main contribution to the electrical process, which results in the phenomenon of $\mathrm{d}R/\mathrm{d}I < 0$. Therefore, the anomalous R–I behaviours again indicate that the hopping and tunnelling effects in the samples are much stronger than those of the other film systems.

We find in figure 6 that R (as well as R_0) decreases after the first R–I measurement and the R–I relation corresponds to an irreversible behaviour. This experimental result is reasonable since, whenever a weak link reaches the melting temperature, the weak link may be either broken down or improved (become wider). In both cases the local microstructures are changed and therefore the irreversible I–V behaviour occurs. The relative change of the resistance $\Delta R/R$, which increases with the resistance R_0, in figure 6 is about 35 and 2% (inset), indicating that, for a certain current, the microstructure of the films with high resistance changes much more than that of the samples with low resistance. As mentioned above, the thinner the sample is, the more defects (like MIM tunnelling junctions) will exist in the film. Therefore, the higher the sheet resistance, the larger the relative change of the resistance $\Delta R/R$ will be. Since R and R_0 decrease for the weak links improve and for the breakdown of the tunnelling junctions.

Because of the hopping and tunnelling effects, it is difficult to obtain the dependence of the breakdown current I_c on the resistance R_0 from the R–I characteristics directly. However we find in figure 7(a) that the critical current I_m depends on the film thickness, i.e., the resistance R_0. The scaling of I_m as a function of R_0 is shown in figure 7(b). The measurements provide a wide span of resistance R_0 and critical currents I_m: four decades of R_0 and three decades of I_m. We find that, just like the relation between I_c and R_0, I_m and R_0 also satisfy a power-law

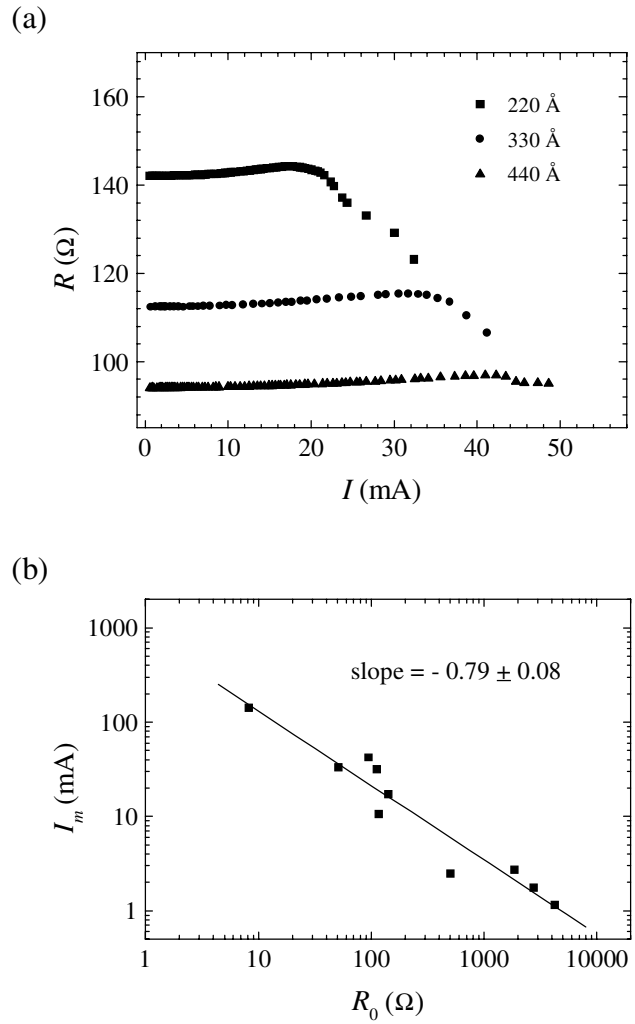

Figure 7. (a) R–I characteristics of three samples with thicknesses of 220 Å (squares), 330 Å (circles) and 440 Å (triangles). (b) Scaling of I_m as a function of the film resistance R_0. The straight line describes the power law $I_m \propto R_0^{-\beta}$, with $\beta = 0.79 \pm 0.08$.

relation, $I_m \propto R_0^{-\beta}$ with $\beta = 0.79 \pm 0.08$. Although the physical origin of this behaviour is still not very clear at the moment, we believe that, just like the exponent α dose [12, 14–16], the new exponent β should be sensitive to the sample microstructure.

The plotting of the critical current I_m as a function of the dc third-harmonic coefficient B_0, as shown in figure 8, yields $I_m \propto B_0^{-\gamma}$ with $\gamma = 0.49 \pm 0.07$. We find that this value of the exponent γ is very close to the theoretical prediction value of the exponent x in equation (4) for the two-dimensional percolation system [14]. This result is reasonable since, just like the relation between I_c and B_0, both I_m and B_0 relate to the local temperature rise. Therefore, we believe that the critical current I_m should be related to the breakdown current I_c and the critical exponent γ, just like the exponent x [14], should be almost insensitive to the sample microstructure and therefore should be universal.

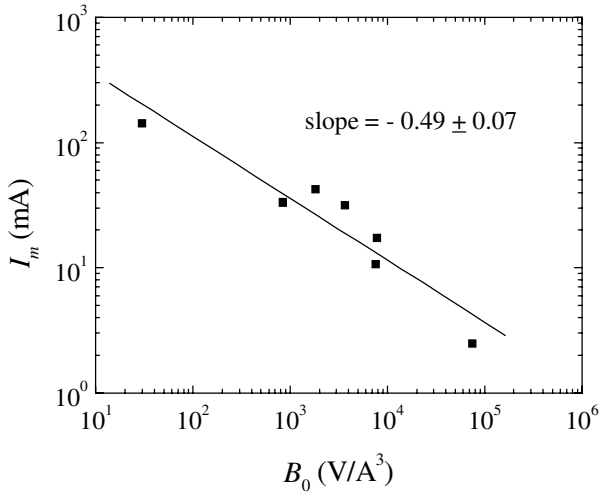

Figure 8. Scaling of I_m as a function of the coefficient B_0. The straight line describes the power law $I_m \propto B_0^{-\gamma}$, with $\gamma = 0.49 \pm 0.07$.

4. Conclusion

In summary, we have studied the surface morphologies and electrical properties of Au films deposited on the silicone oil surfaces. The surface morphologies show that the films exhibit web-shaped and percolation characteristic structures. The dc sheet resistance R of the samples is measured *in situ* during and after deposition by the four-probe method. The dependence of the resistance R on deposition time t can be well interpreted in terms of the film growth mechanism on the oil surfaces. The aggregation time t' dependence of resistance R results from the aggregate characteristics of the Au films, which is similar to the phenomena of the silver films deposited on the silicon oil surfaces [17, 18, 20]. The anomalous I–V behaviour results from the competition among the local Joule heating, hopping and tunnelling effects and indicates that the hopping and tunnelling effects in the samples are much stronger than those of the other film systems [13, 14]. The dc third-harmonic coefficient B_0 and the zero-power resistance R_0 satisfy the power-law relation $B_0 \propto R_0^{2+w}$, where the critical exponent w is close to zero, which is quite different from that of the other films and from the theoretical predications in a two-dimensional system [13]. This result again provides evidence that the hopping and tunnelling effects in the sample are much stronger than those of the other film systems [13, 14]. It is found that the critical current I_m, which corresponds to the maximum resistance, can be well fitted to a power of the resistance R_0 with the exponent $\beta = 0.79 \pm 0.08$. The dependence between I_m and B_0 satisfies the power-law relation $I_m \propto B_0^{-\gamma}$ with $\gamma = 0.49 \pm 0.07$, which is very close to the theoretical prediction value of the exponent x for the two-dimensional percolation system [14]. We believe that the critical current I_m should be related to the breakdown current I_c and the exponent γ, like the exponent x [14], should be almost insensitive to the sample microstructure and therefore should be universal.

The results above show us that the liquid substrate has various influences on the electrical properties of the metal films though further research on the physical origins of these effects is still needed. We believe that other behaviours of the samples, such as magnetic properties, optical properties etc, will exhibit many unusual physical characteristics since the nature of the liquid substrate is quite different from that of the solid one. Further experimental and theoretical research on this topic is now in progress.

Acknowledgments

The financial support from the National Natural Science Foundation of China (grant No 10174063), the Special Foundation for Young Scientists of Zhejiang Province, China (grant No 1997-RC9603) and the Foundation of the Ministry of Education, Zhejiang Province, Chian (grant No 20020757) is gratefully acknowledged.

References

[1] Lewis B and Anderson J C 1978 *Nucleation and Growth of Thin Films* (New York: Academic)
[2] Zhang Z Y and Lagally M G 1998 *Morphological Organization in Epitaxial Growth and Removal* (Singapore: World Scientific)
[3] Sandomirskii V B 1967 *Zh. Eksp. Teor. Fiz.* **53** 1218
[4] Nishiura N, Yoshida S and Kinbara A 1973 *Thin Solid Films* **15** 133
[5] Haus J W and Kehr K W 1987 *Phys. Rep.* **150** 263
[6] Laibowitz R B and Gefen Y 1984 *Phys. Rev. Lett.* **53** 380
[7] Song Y, Lee S I and Gaines J R 1992 *Phys. Rev.* B **46** 14
[8] Ye G X, Wang J S, Xu Y Q and Zhang Q R 1993 *Solid State Commun.* **88** 275
[9] Ye G X, Xu Y Q, Ge H L, Jiao Z K and Zhang Q R 1995 *Phys. Lett.* A **198** 251
[10] Krim J, Heyvaert I, Van Haesendonck C and Bruynseraede Y 1993 *Phys. Rev. Lett.* **70** 57
[11] Ye G X, Wang J S, Xu Y Q, Jiao Z K and Zhang Q R 1994 *Phys. Rev.* B **50** 13 163
[12] Ye G X, Zhang Q R, Feng C M, Ge H L and Jiao Z K 1996 *Phys. Rev.* B **54** 14 754
[13] Yagil Y and Deutscher G 1992 *Phys. Rev.* B **46** 16 115
[14] Yagil Y, Deutscher G and Bergman D J 1992 *Phys. Rev. Lett.* **69** 1423
[15] de Areangelis L, Redner S and Herrmann H J 1985 *J. Physique Lett.* **46** 585
[16] Bowman D R and Stroud D 1989 *Phys. Rev.* B **40** 4641
[17] Ye G X, Michely Th, Weidenhof V, Friedrich I and Wuttig M 1998 *Phys. Rev. Lett.* **81** 622
[18] Michely Th, Ye G X, Weidenhof V and Wuttig M 1999 *Surf. Sci.* **432** 228
[19] Ye G X, Xia A G, Gao G L, Lao Y F and Tao X M 2001 *Phys. Rev.* B **63** 125405
[20] Yang B, Scheidtmann J, Mayer J, Wuttig M and Michely T 2002 *Surf. Sci.* **497** 100
[21] Fujiki Y 1959 *J. Phys. Soc. Japan* **14** 1308